CHAPTER-2

Material, Methodology

And

Characterization Techniques

EXPERIMENTAL TECHNIQUES

2.1 Overview

This chapter provides a comprehensive overview of the experimental procedures utilized to synthesize the materials used in this study and a detailed explanation of the basic principles behind the experimental techniques and protocols. Nevertheless, every chapter encompasses a distinct concept. The fundamental elements and procedures used in each chapter will be explicitly explained within the confines of that particular chapter.

2.2 Materials and Methods:

This section presents comprehensive information on the materials used in this study, including their sources and the precursors employed. This section also provides specific information on their synthesis techniques.

Figure 2.1 Globar Furnace used for melting.

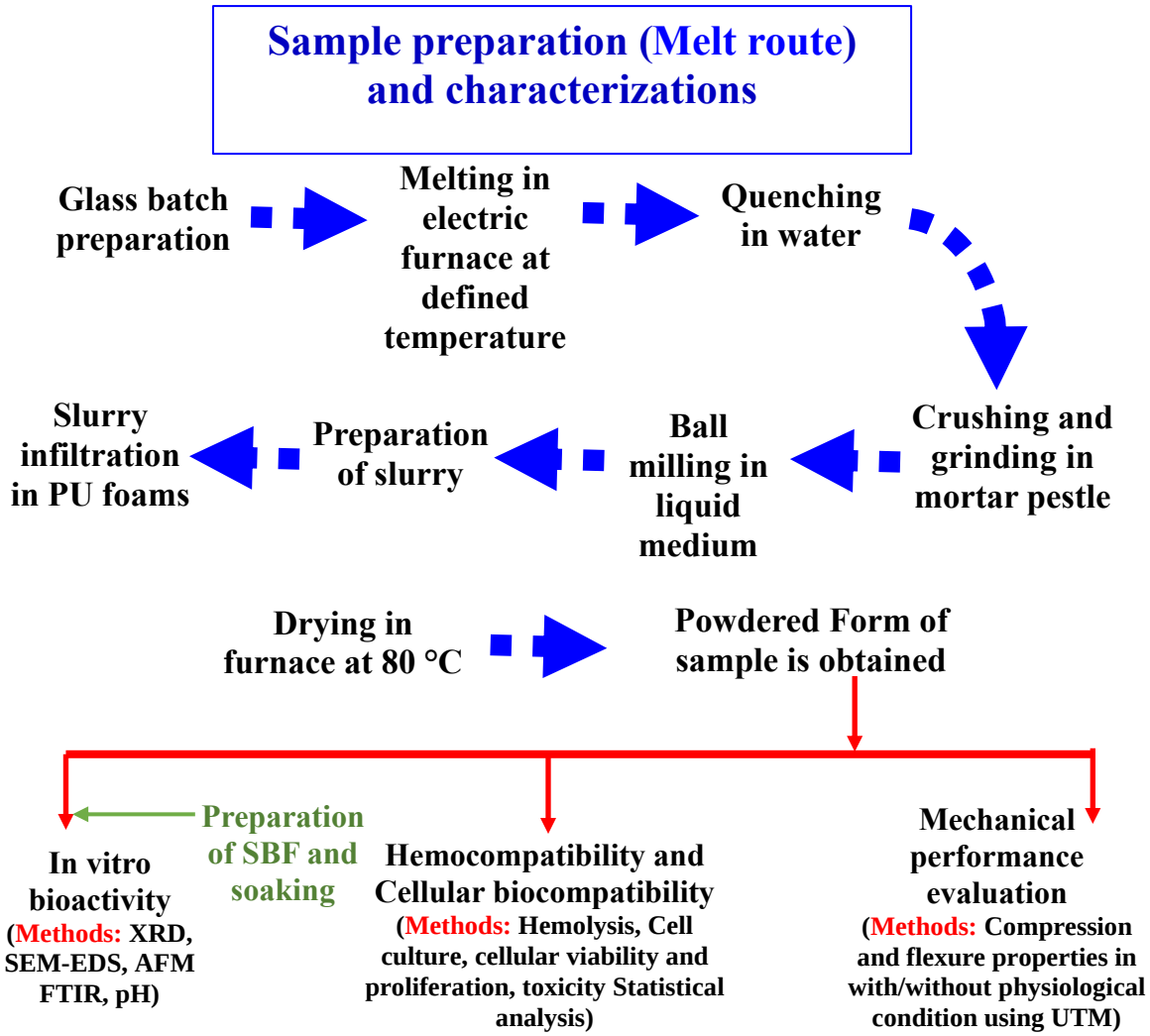

Figure 2.2 Steps for Solid-State Technique and further characterization.

2.2.1 Materials Preparation:

The production of bioactive glass nanoparticles included the consecutive steps of the solid state technique, as shown in the Figure 2.2. The process requires sample preparation, dehydration, and high-temperature treatment. The weight of each precursor used in each composition was calculated by multiplying the weight of the precursor by its corresponding molar weight. This process was repeated for each precursor used to find the number of moles of each precursor needed for the desired glass composition.

$$\mathbf{Wa} = \frac{XaZa}{\sum_{i=1}^{n} XiZi} \qquad \text{.....(ii)}$$

Here, Wa = Weight fraction, Xa = Mole fraction, Za = Molecular weight of oxide

All the materials are purchased from Loba Chemicals. They are taken and calculated according to equation (ii).

Table 2.1 Weight % composition of V_2O_5 substituted Borosilicate glass.

Chemicals	V1	V2	V3	V4	V5	V6	V7
SiO_2	74	73.9	73.7	73.5	73	71.5	70
Na_2O	16	16	16	16	16	16	16
B_2O_3	10	10	10	10	10	10	10
V_2O_5	0	0.1	0.3	0.5	1	2.5	4

Table 2.2 Weight % composition of V_2O_5 substituted 1393-B3 Borate glass.

Chemicals	1393-B3	Vb1	Vb2	Vb3	Vb4
B_2O_3	53	52	51.5	51	50.5
CaO	20	20	20	20	20
Na_2O	6	6	6	6	6
P_2O_5	4	4	4	4	4
MgO	5	5	5	5	5
V_2O_5	0	1	1.5	2	2.5
K_2O	12	12	12	12	12

Table 2.3 Weight % composition of TiO_2 substituted 1393-B3 Borate glass.

Chemicals	1393-B3	BG1	BG2	BG3	BG4
B_2O_3	53	52	51.5	51	50.5
CaO	20	20	20	20	20
Na_2O	6	6	6	6	6
P_2O_5	4	4	4	4	4
MgO	5	5	5	5	5
TiO_2	0	1	1.5	2	2.5
K_2O	12	12	12	12	12

Table 2.4 Weight % composition of ZrO_2 substituted 1393-B3 Borate glass.

Chemicals	1393B3	BZ1	BZ2	BZ3	BZ4
B_2O_3	53	52	51.5	51	50.5
CaO	20	20	20	20	20
Na_2O	6	6	6	6	6
P_2O_5	4	4	4	4	4
MgO	5	5	5	5	5
ZrO_2	0	1	1.5	2	2.5
K_2O	12	12	12	12	12

Table 2.5 Mole% composition of ZnO substituted 45S5 glass.

Chemicals	ZBG0	ZBG1	ZBG2	ZBG3	ZBG4	ZBG5
SiO_2	46.1	46.1	46.1	46.1	46.1	46.1
Na_2O	24.4	23.4	22.9	22.4	21.9	21.4
CaO	26.9	26.9	26.9	26.9	26.9	26.9
P_2O_5	2.6	2.6	2.6	2.6	2.6	2.6
ZnO	0	1	1.5	2.0	2.5	3

The glass samples weight taken corresponding to the glass selected for the preparation. As shown in the following tables the different compositions taken for glass preparation. Tables 2.1 to 2.5 show the different compositions used for glass preparation. These tables show three different types of glasses doped with four distinct transition metals as shown in the Tables.

2.2.1.1 Melting:

Once the batch was prepared, it was transferred into a platinum crucible. The platinum crucible was cleaned by immersing it in hydrochloric acid. Subsequently, the crucible-containing sample system was inserted into the electric furnace. A platinum lid was used to cover the sample containing the crucible to prevent moisture contact during glass melting. The temperature of each batch was raised to the specific level required for the corresponding kind

of glass, i.e. 1400°C for transition metal substituted borosilicate glass and 45S5 glass, 1100°C for transition metal substituted 1393-B3 borate glass. We take safety procedures in handling quenching method like using the Personal Protective Equipment (PPE) including safety gloves: safety Glasses, safety Shoes and heat-resistant clothing. Figure 2.3a shows a picture of glass melting. Only the colour yellow can be seen here. We must look at the crucibles through cobalt blue glasses to locate them and taken them out for pouring them in steel mould (Figure 2.3b). After that, it was put into stainless steel plate dies and subjected to annealing processes.

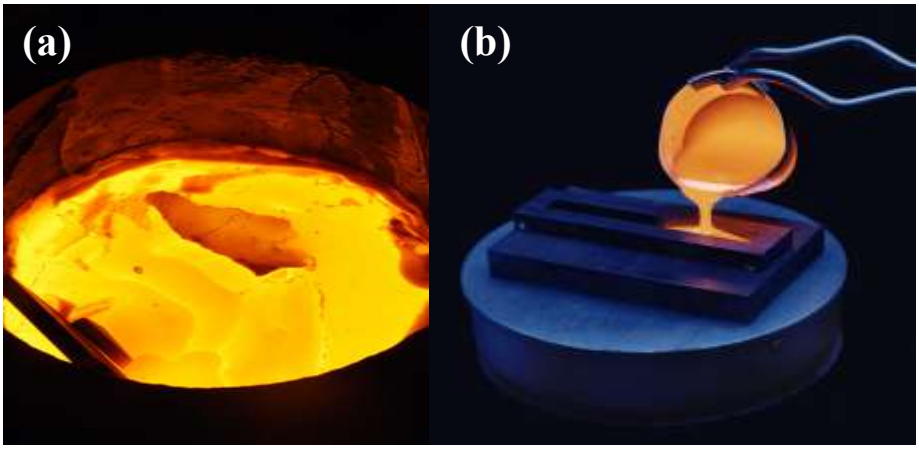

Figure 2.3 (a) Glass Melting **(b)** Melted glass samples casted in steel mould.

2.2.1.2 Annealing:

Glass annealing is the method of gradually cooling heated glass items after their formation to alleviate any remaining internal tensions created during the manufacturing process. The process of annealing glass is crucial for enhancing its durability. Insufficiently annealed glass preserves thermal stresses resulting from rapid cooling, leading to a permanent reduction in the strength and dependability of the product. Glass that has not been adequately annealed is prone to cracking or shattering when exposed to minor fluctuations in temperature or when subjected to mechanical shock or stress.

2.2.1.3 Granulation and pellet processing:

The powder resulting from the calculation was uniformly blended by grinding it with a pestle in an agate mortar. Subsequently, a 2% solution of polyvinyl alcohol (PVA) with the

powder until it reached a fine consistency. The fine powder was pelletized using a hydraulic press and a die with a diameter of 10 mm, exerting pressure. The resulting pellet is then used for further characterization.

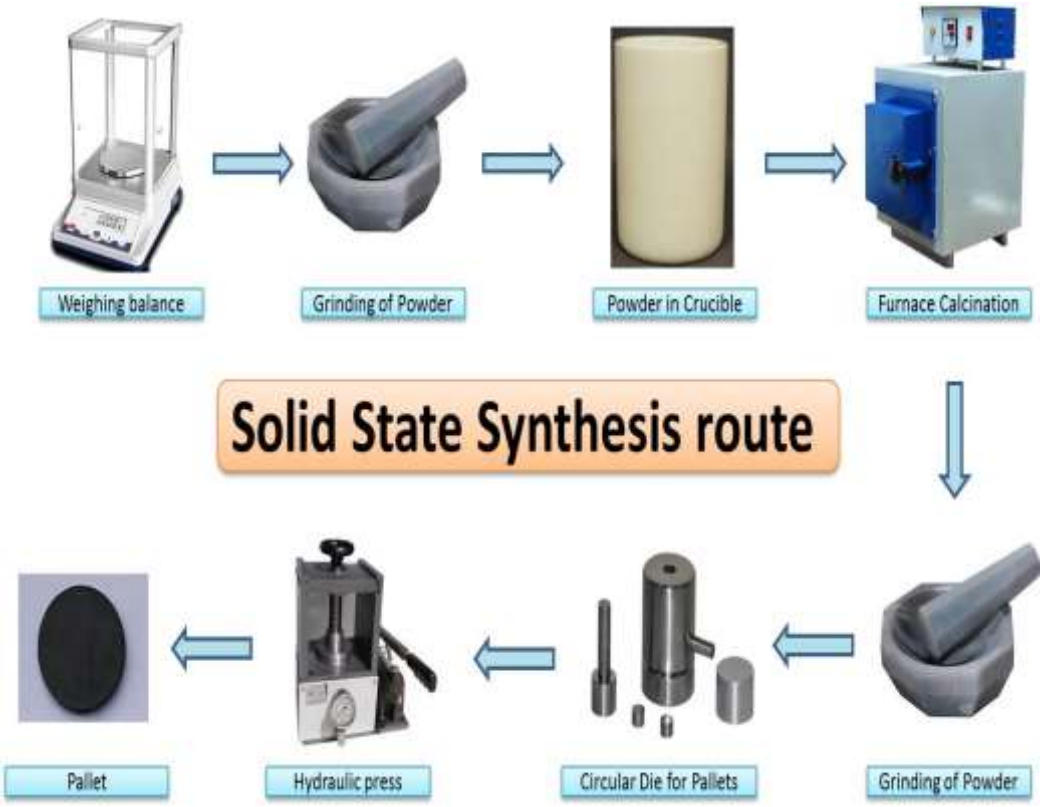

Figure 2.4 Schematic diagram for preparation of pallets through Solid-State Synthesis route.

The pallets underwent a heat treatment process where they were exposed to a specified temperature depending on glasses for a duration of 8 hours. The heating and cooling of the products occurred at a rate of 2°C per minute, starting at room temperature. Additional characterization methods were used to analyze the development of pellets' phases, microstructure, and electrical and mechanical characteristics.

2.3 Materials Characterization techniques

The two following sections delineate the pertinent methodologies used to characterize the samples. The fundamental ideas behind each strategy will be concisely explained, and any relevant material will be provided in the appendices.

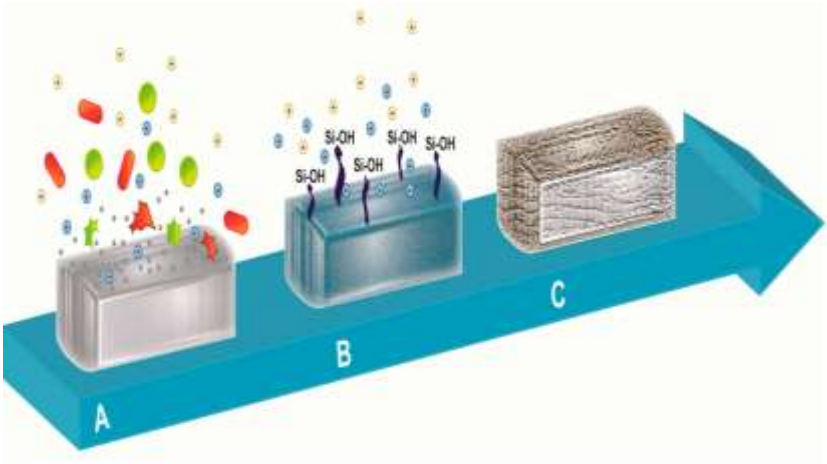

Figure 2.5 Schematic representation of the reaction upon body fluids contact. (Lorenzo et al.).

2.3.1 Physical Properties (Measurement of Density):

The density of bioactive glass samples was determined using Archimedes' principle, with distilled water as the buoyant medium. The weight measurements were conducted using a digital balance (Figure 2.6) with a precision of ± 0.0001 g. The density value calculated according to the Archimedes' principle.

Archimedes' principle states that the buoyant force imposed on an object submerged in a fluid, whether wholly or partly, is equal to the weight of the fluid displaced by the object. This force works in the upward direction at the centre of mass of the displaced fluid.

Here, the sample is immersed in the buoyant, and then the weight of the samples is measured before and after the immersion of the sample in the buoyant liquid.

Therefore, the density of the glass sample may be expressed as:

$$\boldsymbol{\rho = \frac{w_a}{\omega_a - \omega_b} \rho_b} \text{.....(iii)}$$

Here, w_a = Weight of the sample in air, w_b = Weight of the sample in buoyant, ρ_b = Density of buoyant

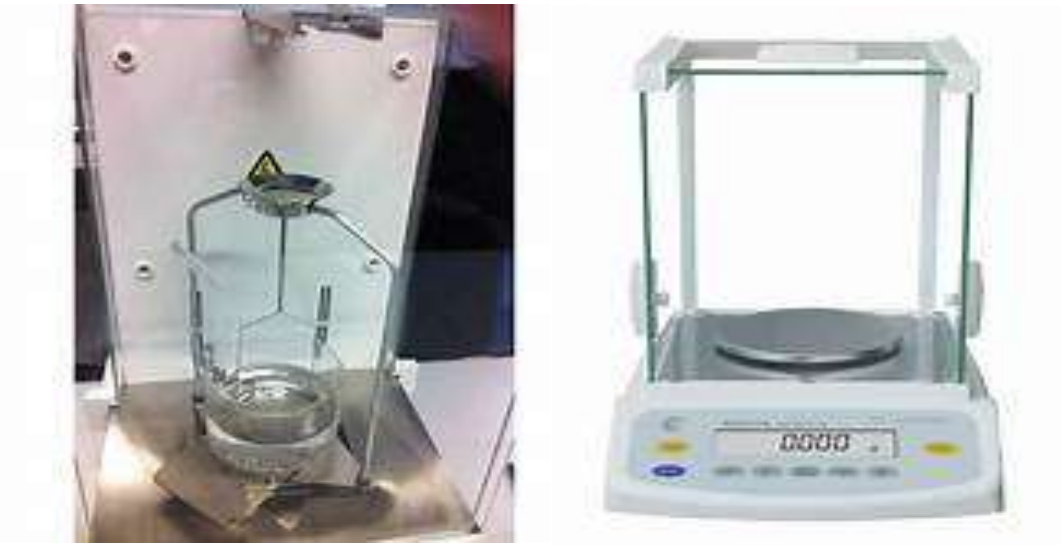

Figure 2.6 Density measurement instrument [Sartorius BSA2245CW] **(a)** Density kit **(b)** Balance.

2.3.2 Chemical Properties (pH Measurement):

Examining changes in solution pH when bioactive glasses are dissolved in simulated bodily fluids is crucial. The measurement of pH values may be conveniently performed with a pH meter, which consists of a glass probe containing two internal electrodes. One electrode is immersed in a liquid with a constant level of acidity, whereas the pH of the sample solution influences the response of the second electrode. When converted into a pH value, the voltage difference between the two electrodes yields a result of 42. This conversion is accurate if the instrument was calibrated before the test. The pH testing machine is shown in Figure 2.7.

Figure 2.7 Microprocessor based pH meter.

2.3.3 Mechanical Properties:

A compression experiment was performed to ascertain the stress and strain of all composites. Stress may be defined as the immediate force exerted on a specimen, divided by its cross-sectional area (Roeder, 2013). Compression testing involves applying stress to the sample, causing it to deform in the direction that applies the stress. The recorded result of the test is the force applied divided by the change in sample length. Three specimens of each composition were used to quantify the compressive strength. The results were averaged. The composite samples were produced by shaping them into cylindrical pallets measuring $10^5 mm^2$ before undergoing the sintering process. The samples were meticulously prepped to ensure that both sides were free from cracks and perfectly parallel. The specimens were subjected to compression using the Tinius Olsen HIOKL Universal Testing Machine at a 0.5 mm/min crosshead speed. The tension was determined using equation. The force applied to an object that results in compressive stress is directly related to the cross-sectional area of the object.

(i) Compressive Strength: The inherent capacity of a system or substance to withstand loads that impose a force to lower the material's dimensions is referred to as compression strength. This property is also known as compressive strength. The compressive strength (σ) of the bioactive glass is calculated with the formula:

$$[\ \sigma = F/\ \pi r^2\ ]\text{……..(iv)}$$

(ii) Flexural Strength: The strength of a material is often defined as the maximum amount of stress during bending that may be applied to the substance before it experiences any kind of mechanical deformity. This strength is known as Flexural strength.

$$\textbf{Flexural strength (MPa)} = \frac{3\times F\times l}{2\times b\times h^2} \text{……..(v)}$$

Where, F=load in Newton, l=length b=width h =thickness of the pallet

(iii) Elastic Properties Measurement:

The velocities of longitudinal and shear ultrasonic waves for Titanium-doped 1393-B3 are being measured. The bioactive and base glass was quantified using the Olympus equipment (M-45, USA). The glass sample was cut and polished into cubic pieces, from which velocities were measured. The elapsed time between the commencement and the reception of the pulse displayed on the screen of an ultrasonic defect detector was measured using a standard electrical circuit.

Figure 2.8 Olympus instrument (M-45, USA).

The elastic properties have been determined using longitudinal and tangential velocities:

1. Poisson's Ratio (υ)

$$\boldsymbol{\nu = \frac{V_L^2 - 2V_T^2}{2(V_L^2 - V_T^2)}} \quad \textbf{.....(vi)}$$

2. Young's Modulus (E)

$$\boldsymbol{E = \frac{\rho V_L^2 (3V_L^2 - 4V_T^2)}{V_L^2 - V_T^2}} \quad \textbf{.....(vii)}$$

3. Bulk Modulus (K)

$$\boldsymbol{K = \frac{1}{3}\rho(3V_L^2 - 4V_T^2)} \textbf{.....(viii)}$$

4. Shear Modulus (G)

$$\mathbf{G = \rho V_T^2} \quad \textbf{……(ix)}$$

Here, V_L = Longitudinal Velocity, V_T= Tangential Velocity, ρ=Density

2.3.4 Thermal analysis (DSC-TGA):

The DSC-TGA instrument has an experiment unit equipped with two alumina crucibles, one for retaining the sample and the other for serving as a reference. The sample is subjected to heating by a pre-established temperature profile. The change in mass is quantified as a function of temperature, while the difference in temperature between the sample and the reference material is measured simultaneously. Throughout the experiment, the reference material remains constant in its thermal properties and does not disrupt the characteristics of the tested gas. A change in the physical parameters of the sample causes a temperature difference between the sample and the reference. Crystallization is linked to exothermic reactions, whereas freezing is related to endothermic reactions.

Figure 2.9 DSC/TGA Instrument.

Thermo-gravimetric analysis (TGA) is a method used to ascertain the temperature at which a sample undergoes calcination and assess the stability of materials. This study records

the variation in mass of the experimental sample as a function of temperature. This data gives insight into the processes of mass gain (absorption), mass loss (desorption), phase transition, and other related phenomena of the sample (Cammenga et al., 1995). A sample is considered thermally stable within a specific temperature range if its mass stays consistent. TGA also offers data on the maximum temperature at which the sample begins to degrade. TGA, or thermos-gravimetric analysis, is often used in literature to determine the sample's reaction temperature and the stability of materials, among other factors. Differential scanning calorimetry (DSC) is a technique that quantifies the difference in heat-flow rate between a sample and a reference sample while they undergo a controlled temperature program.

The established weight sample undergoes heating or cooling, and variations in heat flow measure the alteration in heat capacity. Using this methodology, one may deduce the specific kind of reaction (either endothermic or exothermic) and determine the enthalpy, Gibbs energy, and other thermal characteristics. The simultaneous thermogravimetric analysis (TGA) and differential scanning calorimetry (DSC) provide insights into the reaction route of the created combination of raw materials. It also allows for identifying key transition points such as the melting point, glass transition temperature, and crystallization temperature (Huang et al., 2016). The DSC-TGA measurement was conducted using the DSC-TGA (Mettler Toledo, Germany) model shown in Figure 2.9, operating in a temperature range of 27°C-1000°C in a nitrogen gas environment.

2.3.5 Electrical Property Analysis (Dielectric Measurement):

The configuration we use to measure the dielectric is shown in Figure 2.10. The setup comprised a sample holder placed into a divided furnace. The sintered pellets underwent a process in which they were covered with silver paste and then subjected to a temperature of 500 °C for 30 minutes. The dielectric measurements were conducted using an Autolab

potentiostat, varying the frequency from 1 MHz to 1 Hz and at various temperatures. The measurements were recorded only during the cooling phase.

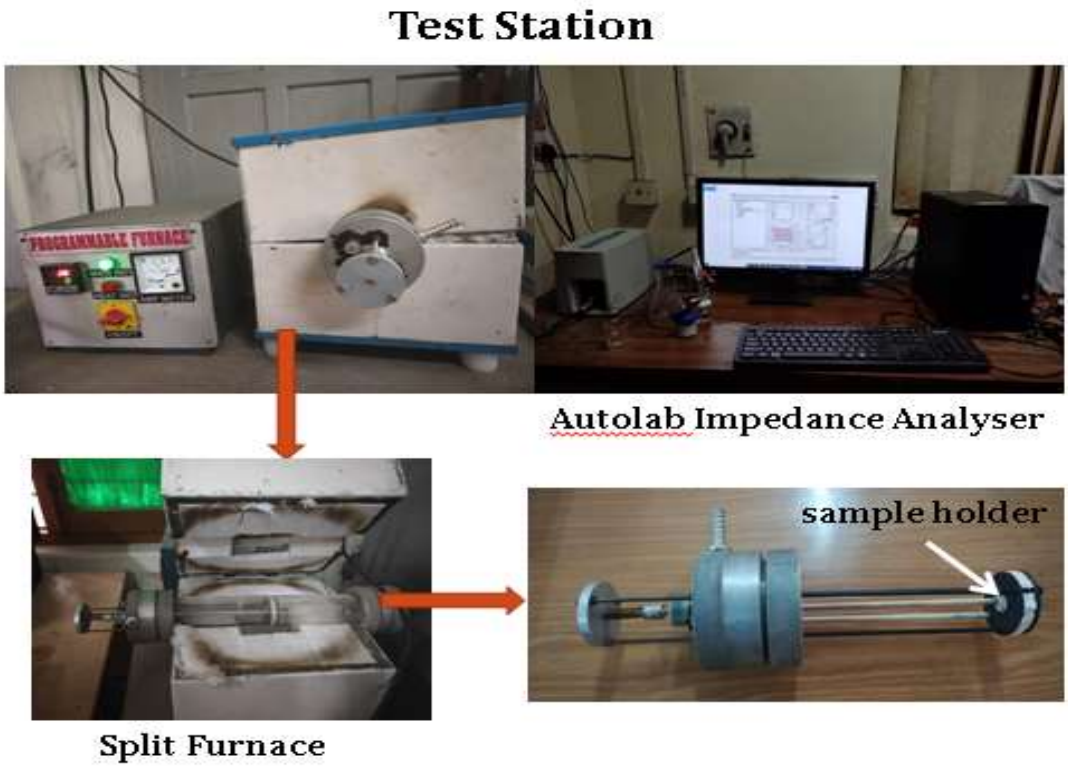

Figure 2.10 Schematic representations Dielectric Test station.

The impedance spectroscopy was conducted at several temperatures under ambient conditions to investigate the dielectric properties of the material. The dielectric constant was determined by using the formula:

$$\varepsilon_r = \frac{C * d}{\varepsilon_\circ * A} \qquad \text{..... (x)}$$

Here, the dielectric constant (εr), capacitance (C), permittivity of free space (εo), thickness of the pellet (d), and area of the pellet (A). The permittivity of free space is represented as 8.85*10-12 F/m. Capacitance (C) was calculated by using the formula

$$C = -\frac{1}{\omega}\left[\frac{Z''}{Z'^2 + Z''^2}\right] \text{..... (xi)}$$

and the dielectric loss was calculated with the following equation

$$\tan\delta = \frac{\varepsilon''}{\varepsilon'} = \frac{Z'}{-Z''} \text{..... (xii)}$$

2.3.6 In vitro bioactivity studies:

The biological function of biomaterials is assessed by soaking them in simulated bodily fluid (SBF). The primary criterion for determining bioactivity is hydroxyapatite deposition onto the surface. The formulation of SBF was specially designed to achieve the ionic concentrations shown in Table 1.2, which nearly mimic the ionic concentration seen in blood plasma.

SBF is formulated using the established methodology developed by Kokubo et al. in 2006. This involves dissolving several compounds, as listed in Table 2.6. To prepare a 1000 mL solution of simulated body fluid (SBF), fill a meticulously cleaned HDPE beaker with 750 mL of deionized water. Stir the mixture at a temperature of 37°C. Subsequently, the compounds were sequentially incorporated in the precise sequence shown in Table 2.6. Every ingredient was allowed to mix until fully dissolved before adding the next chemical. The tris-buffer [(CH_2OH), CNH_2] was added cautiously to avoid an abrupt increase in the solution's pH. The final pH of SBF was adjusted to 7.40 using IM HCI at a temperature of 37°C. Subsequently, the solution was diluted to a volume of 1000 ml using deionized water and then chilled to the ambient temperature before being kept in a refrigerator. The bioactive glass powders were immersed in a simulated body fluid (SBF) for 2, 5, 7, 14, 21, and 28 days. The immersion took place in an incubator set at a temperature of 37°C. The ratio of SBF to powder was maintained at a ratio of 100:1. To ascertain the pH of the solution; the powders were removed from the solution after a predetermined amount of time had passed during the immersion process. After that, the wet powders were subjected to a drying process in a hot oven at 70°C for 48 hours. X-ray diffraction (XRD), Fourier transform infrared spectroscopy (FTIR), Atomic Force Microscopy (AFM) and Scanning electron microscopy - Energy-dispersive X-ray spectroscopy (SEM-EDS) techniques were used to investigate the formation of a hydroxyapatite layer on the surface of these samples.

Table 2.6 Chemicals used for the preparation of simulated body fluid (SBF).

S. NO.	Chemical	Quantity
1.	NaCl	7.996g
2.	$NaHCO_3$	0.350g
3.	KCl	0.224g
4.	$K_2HPO_4.3H_2O$	0.228g
5.	$MgCl_2.6H_2O$	0.305g
6.	HCl	40 cm^3 with a concentration of 11kmol/m^3
7.	$CaCl_2$	0.278g
8.	$NaSO_4$	0.071g
9.	$(CH_2OH)CNH_2$	6.057g
10.	HCl	as much as is required to change the pH with a concentration of 1kmol/m^3.

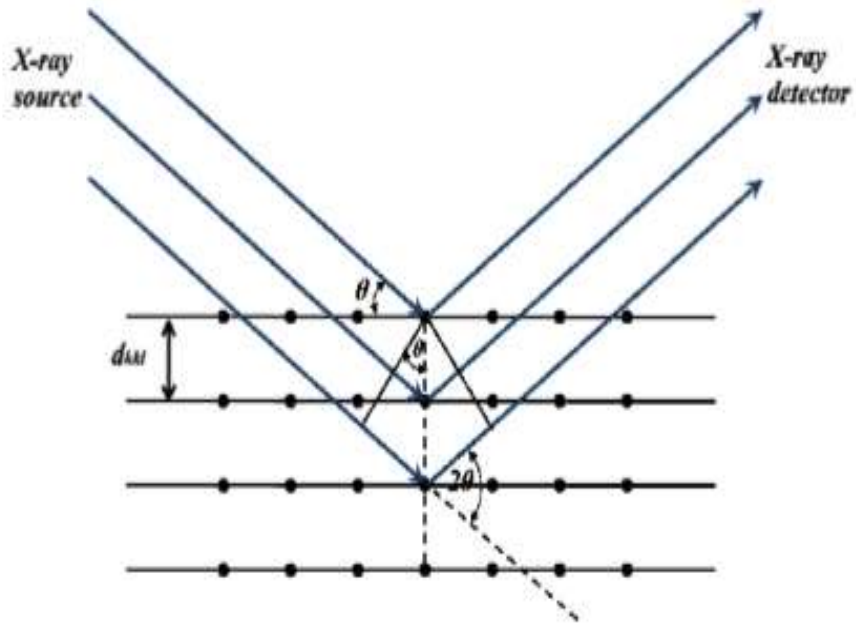

Figure 2.11 Demonstration for Bragg's Law.

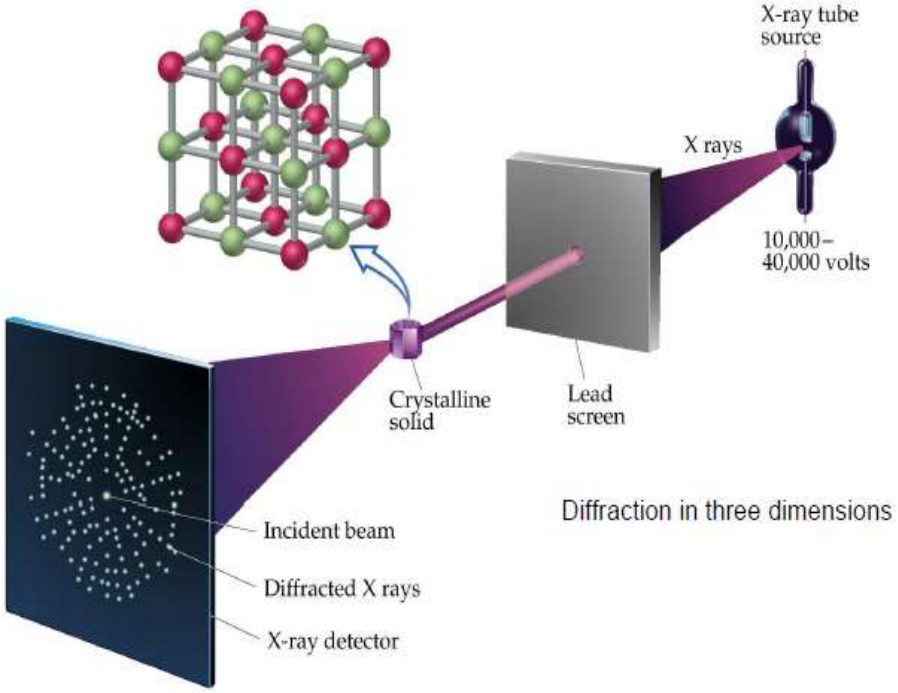

Figure 2.12 Principle of XRD.

Figure 2.13 X-Ray Diffractometer Instrument.

2.3.6.1 Phase Formation and Crystal Structure Studies by XRD:

X-ray diffraction (XRD) is a flexible and fundamental method for identifying the phases of a substance. It has been widely used and recognized for many years. The term "powder X-ray diffraction" refers to a method that involves analyzing the XRD pattern obtained from a densely packed powder sample. The powder samples consist of several minute polycrystals with randomly oriented domains in all conceivable orientations, which leads to the formation of the XRD pattern. Coherently diffracting domains refer to the specific domains that produce diffraction in the same direction. This method is used to ascertain the crystal structure, favoured alignment of lattice planes, dimensions of crystallites, and the distribution of shapes and sizes in a polycrystalline powder (Prabhu et al., 2014). This non-destructive approach allows for collecting diffraction patterns while subjecting the samples to various pressure and temperature conditions. X-ray diffraction is a method used to identify the crystalline phases of a substance by using monochromatic X-rays. Diffraction happens when a wave interacts with a lattice with a uniform spacing equal to the wavelength of the X-rays. X-rays are used to examine crystallographic structures because their wavelength is comparable to the atomic spacing of various materials. This similarity enables the occurrence of diffraction, resulting in the formation of constructive and destructive interference patterns of the X-rays. As shown in Figure 2.11, the diffraction satisfies the Bragg equation:

$$2dsin\theta = n\lambda \quad \text{..... (xiii)}$$

Here, d is the distance between beams that are diffracting, is the angle at which the beam is incident, n is an integer, and λ is the wavelength of the beam.

The XRD data were collected using a step scan mode at a low scanning rate. The principle of XRD explained in Figure 2.12. The various crystallographic phases of the current sample were determined by analyzing the X-ray diffraction pattern at room temperature. This was done using an X-ray diffractometer (Rigaku Miniflex II, Japan- Figure 2.13) equipped with

Cu Ka radiation with a wavelength of 1.5418 A. The diffractometer operated at an applied voltage of 40 kV and a current of 40 mA. The XRD pattern was obtained by scanning in the angular range of 20.80° with a step size of 0.02° and a scanning rate of 0.02° per minute. The central divergence slit had a width of 0.6 mm, while the secondary detector had a slit width of 1.0 mm for X-ray diffraction studies. The X-ray diffractometer used for the current thesis research is shown in Figure 2.13. In this experiment, composite samples were created, changed, and then crushed and ground into a fine powder before conducting XRD analysis.

Figure 2.14 FTIR Spectrometer Instrument.

2.3.6.2 Fourier Transform Infrared Spectroscopy (FTIR):

Infrared spectroscopy is a crucial analytical method that allows for the investigation of materials by providing a unique identifying characteristic, sometimes referred to as the "fingerprint," of the samples under study. The instrument shown in Figure used to evaluate the data. The FTIR peaks relate to the absorption of vibrations between the atomic bonds that contribute to the construction of the materials. Each substance has a unique arrangement of atoms, and no two compounds have the same infrared spectrum.

IR spectroscopy may be used to qualitatively analyze and identify many types of materials (Titus et al., 2019). Figure 3.5 displays a schematic diagram illustrating the Fourier transforms infrared (FTIR) spectroscopy process. The FTIR is favoured above other methods of infrared spectrum analysis for the following reasons:

1. This approach is non-destructive.
2. The approach offers an accurate measuring technique that does not need external calibration.
3. It can enhance the data acquisition rate and perform a scan per second.
4. It can handle more optical throughput.
5. It has a simple mechanical design with only a single moving component.

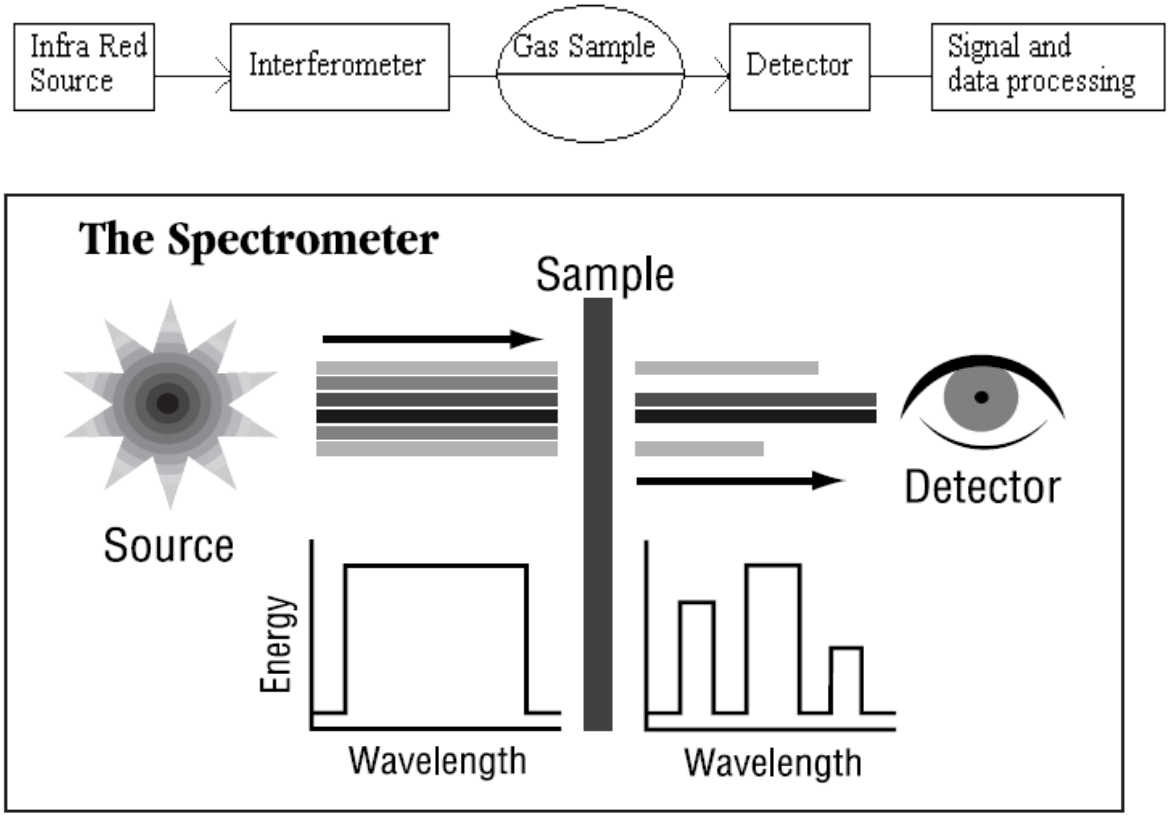

Figure 2.15 Principle of FTIR.

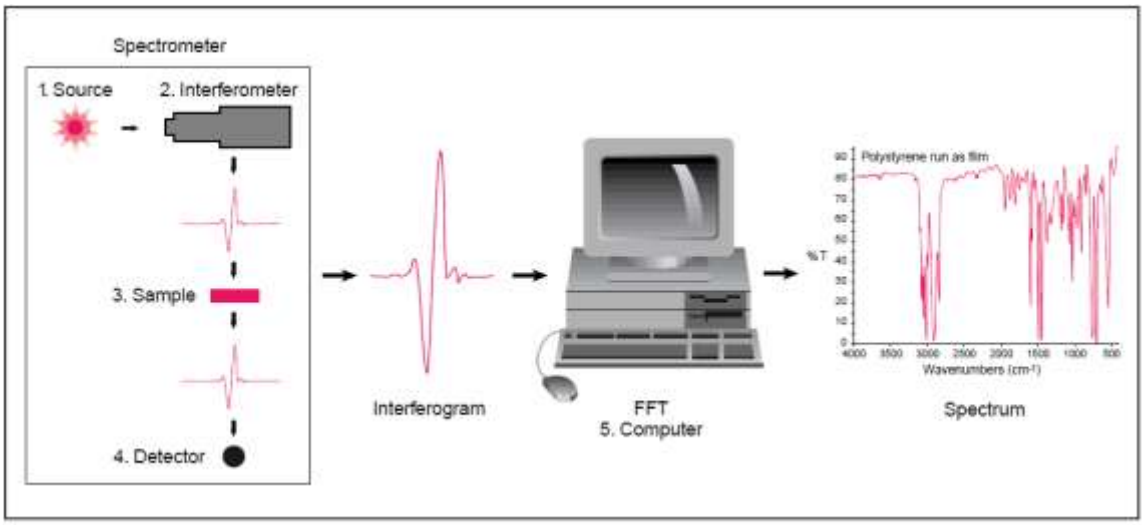

Figure 2.16 Working of FTIR.

FTIR involves the interaction of a beam of light with varying frequencies with a sample. This contact stimulates and causes vibrations in the dipole moments of covalent bonds (Figure 2.15). The intensity of light after the detector then detects this interaction. The interferogram undergoes a Fourier transform to calculate the quantity of light absorbed at each specific wavelength. The data set may be acquired using the reflected, absorbed, or transmitted method working shown in Figure 2.16.

The energy of the bonds use is governed by the particular kind of bonds present, which in turn leads to the formation of a distinct spectrum (Berthomieu et al., 2009). The composites used in this study were examined using FTIR spectroscopy before and after being immersed in simulated body fluid (SBF) to assess any potential alterations in their bioactivity. The materials were pulverized into a fine powder, and the spectra were measured with a resolution of $2cm^{1}$, covering a range from 400 to 4000 cm.

The data were gathered using an FTIR instrument (JASCO FTIR 4600 etc.) in transmission mode with attenuated total reflectance (ATR) mode.

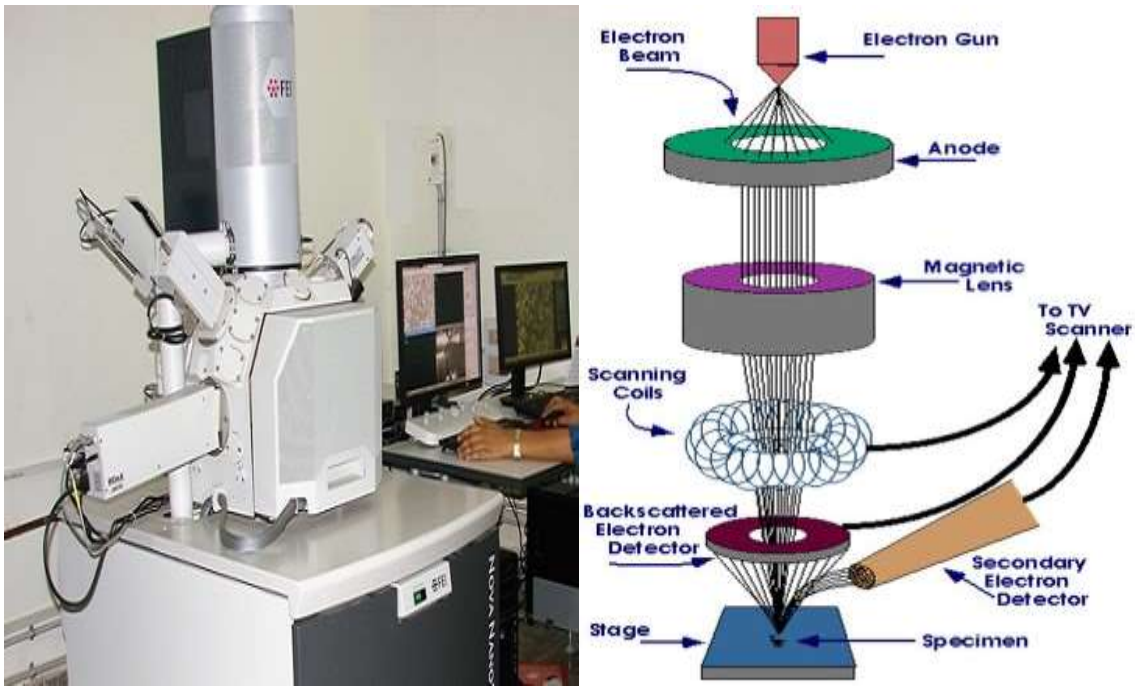

Figure 2.17 (a) SEM-EDS Instrument **(b)** Schematic diagram of SEM.

2.3.6.3 Scanning Electron Microscopy (SEM):

Microstructure and Elemental Analysis of the samples are done with the help of SEM technique. An emitting cathode in the electron gun of a scanning electron microscope produces a narrower beam at both low and high electron energy levels. This leads to enhanced spatial resolution and less sample charging and damage (Goldstein et al., 2017). The electrons were produced by applying a field gradient in a vacuum. The electron beam passed through electromagnetic lenses, focussing it onto the specimen. This interaction resulted in the formation of several kinds of electrons. The detector determines the secondary electron and generates a picture of the surface sample by comparing the intensities of secondary electrons with the principal electron beam. Ultimately, the picture is shown on a monitor equipped with a Field Emission Scanning Electron Microscope (FESEM). The materials in this thesis were imaged using the EVO18 scanning electron microscope (SEM) from Zeiss, Japan. The instrument pictures may be seen in Figure 2.17a. The process of schematic diagram of SEM explained in Figure 2.17b.

2.3.6.4 Energy dispersive X-ray spectroscopy (EDS) analysis:

Energy Dispersive X-ray analysis, also known as EDS or Energy Dispersive Spectroscopy analysis (EDS), is a non-destructive method used to determine the elemental composition of materials with a sensitivity of 0.5 to 1 atomic per cent. This facility is often connected to electron microscopy instruments such as scanning electron microscopes (SEM) and transmission electron microscopes (TEM). It is used to identify a specimen by analyzing the interaction between a high-energy electron beam and the electrons released from the inner shell of atomic orbitals of the atoms in the sample. The electrons in the outer shell replace the vacuum left by the electrons in the inner shell, resulting in the emission of X-rays.

Therefore, the data related to the components of the samples may be examined based on the energy of the produced X-ray. EDS provided qualitative and semi-quantitative data on the ingredients found in the composition. The elemental compositions of the generated samples were verified EDS using an EDXA spectrometer, as seen in Figure 3.6, which was obtained with the FESEM/EVO18 instrument from Zeiss, Japan. This approach was mainly used to identify the constituents inside the tested samples and analyze the changes in the composition of the composite surfaces after immersing the samples in SBF.

Figure 2.18 Atomic force microscopy (NT-MDT equipment).

2.3.6.5 Atomic Force Microscopy (AFM) analysis:

Atomic force microscopy (NT-MDT equipment) was used to evaluate the degraded surface morphologies at a scanning rate of 2μm/s. AFM analysis was used to examine the change in the thickness of produced HA over the ZBG samples after SBF immersion for base and transition metal substituted bioglass samples.

Figure 2.19 Bio-rad iMark™ microplate absorbance reader for cellular analysis.

2.3.7 Biological Evaluation:

Osteoblasts are accountable for the process of bone formation, particularly for the mineralization of the osteoid matrix. The MG 63 cell line was cultivated on the bioactive glass samples to assess the behaviour of the generated networks when exposed to tissues. Human osteoblast-like tissue specimens were regarded as a crucial means for evaluating materials for testing.

2.3.7.1 Cell culture process:

The MG-63 cell line was acquired from the National Centre for Cell Science (NCCS) in Pune, India. The cell line was maintained at 37°C in a humidified incubator with 5% CO_2 and supplied with 10% fetal bovine serum (FBS) and 1× Penicillin/Streptomycin antibiotic.

The MTT test was used to measure cell growth inside the bioactive glass samples. This test relies on the idea that living cells with metabolic activity convert the yellow-coloured tetrazolium MTT into a purple-coloured formazan compound within the cells via the action of the dehydrogenase enzyme. The purple formazan colour was quantified using the spectrophotometric technique after dissolving it in DMSO. The rate at which cells multiply is inversely proportional to the rate at which tetrazolium is reduced. Cell viability was determined using the following mathematical formulas.

$$\textbf{Cell viability}_{\text{sample}}\ \% = \frac{\text{Absample}}{\text{Abcontrol 7 day}} \text{x100} \quad \text{…… (xiv)}$$

$$\textbf{Cell viability control \%} = \frac{\text{Absample}}{\text{Abcontrol 7 day}} \text{x100} \quad \text{…….. (xv)}$$

In this experiment, MG-63 cells were placed on each bioactive glass sample at a concentration of 1×10^6 cells/mL and left to incubate for overnight in a 5% CO_2 incubator to allow for cellular adhesion. To minimize the risk of obtaining inaccurate readings or results caused by cells that had migrated and stuck to the surface of Petri plates, the bioactive glass sample was placed onto 96-well plates for an extended period of culture. The samples were incubated in a 5% CO_2 atmosphere between 2 and 7 days after seeding the cells. The cells cultivated without composites in every well were designated as the positive control, while a complete growth medium was used as the negative control for all tests. Following incubation, the culture media was extracted from every well, and composite materials were then relocated to new, sterile wells to prevent the possibility of erroneous results caused by cells that had migrated and attached to the well's bottom during infection. Each well was treated with a 100 µL solution containing a full growth media (90 µL of DMEM+10%F + 1% PS) and MTT (100 µL of a 5 mg/ml solution in PBS). Following a 4-hour incubation period, the formazan crystals that developed inside the wells were dissolved by adding a 100-microliter solution of dimethyl sulfoxide (DMSO) for 15 minutes. After performing pipette-mixing, the solution was moved

to new wells to prevent any absorbance caused by the scaffold. The optical absorbance was quantified at a wavelength of 570 nm using a multimode microplate absorbance reader shown in Figure 2.19 (Bio-rad iMark™ microplate absorbance reader USA). The MTT test was conducted in triplicate for both cell lines, including positive controls, as described by Varshney et al. (2019). This investigation examined the cell growth rate (viability) in the composites using an MTT test. The cell viability percentage inside the composite was determined based on the absorbance of the positive control measured on day 7.

Figure 2.20 Inverted fluorescence phase contrast microscope.

2.3.7.2 Phase Contrast Imaging:

Through the use of in vitro live cell imaging with a phase contrast microscope, the proliferation of the MG-63 cell line has also been significant. In a nutshell, MDA-MB-231 cells were sown in each well of a 12-well tissue culture plate. Briefly, 50000 MG-63 cells were seeded in each well of 12 well cell culture plate. Then, they were incubated at 37 degrees

Celsius in a humidified environment containing 5% CO_2 for 24 hours. Thereafter, several concentrations of given glass samples were exposed to the cells. These concentrations were 100 µg/ml, 200 µg/ml, 400 µg/ml, 600 µg/ml, and 800 µg/ml individually. Images were captured using an inverted phase contrast microscope (EVOS FL cell imaging system, Life Technologies, USA) shown in Figure 2.20 used at a magnification of 100x after the therapy had been administered for twenty-four hours. These in-vitro images are observed to check the cellular structure at different concentrations of glasses to study cellular confluency. In addition, this proves that the MTT assay was correct.

When taken as a whole, the findings of our cellular compatibility and phase contrast imaging experiments indicate that glass has significant suitability in bone regeneration.

2.3.8 Hemocompatibility:

The hemolytic activity of the composite was assessed using the ASTM F 756-00 technique (ASTM, 2000). To do this, each powder sample was placed into 7 ml of PBS and subjected to incubation at 37°C for 72 hours. After extracting the PBS solution from the sample, 1 ml of diluted blood (9.02 mg/mL) from the human venous blood was added to each sample.

Briefly, Fresh blood was obtained from the vein of the male human hand and placed in tubes coated with heparin, an anticoagulant. The blood was then centrifuged at 650 g for ten minutes at a temperature of 4ºC, and the supernatant was eliminated with caution. The samples were then incubated for 3 hours at a temperature of 37°C. Subsequently, the solution was subjected to centrifugation at a speed of 2000 revolutions per minute for 15 minutes. Following the washing of the red blood cell pellets with cold PBS until the supernatant became transparent, the blood was diluted with PBS at a ratio of 1:10 (blood: PBS). The red blood cell suspension that was produced (0.1 ml) was combined with various products (0.9 ml) at a concentration of 1 mg/ml (in a solution of phosphate-buffered saline). One negative control (no

lysis) and one positive control (100 per cent lysis) were represented by the blank PBS (pH 7.4) and triton x-100, respectively. In order to separate the non-lysed red blood cells (RBCs), the mixture was stored in a shaker incubator at 37 ± 1 ℃ for one hour while being stirred continuously. After that, the mixture was centrifuged at 650 g for ten minutes at 4 °C. Through the use of a microplate reader, the optical density at 540 nm was determined to determine the level of lysis present in the supernatant. The haemoglobin concentration was assessed using hemolysis activity and quantified by measuring the optical densities (O.D.) at 540 nm using a Microplate Reader (Synergy HT Multi-Mode, BioTek, USA). To minimize errors, three copies of each sample were obtained, and their optical density measurements were averaged. The percentage of hemolysis rate was determined using equation (xv) as described by Hossain et al. (2020). The acquired outcomes are being compared to the ASTM standard. The products exhibited a haemolysis rate of less than 4%, as seen in Figure. This haemolysis rate was found to be considerably lower ($p < 0.01$) compared to the positive control group (triton x-100), which was acknowledged to have a crucial haemolytic impact.

$$\textbf{\% Hemolysis control} = \frac{\textbf{O.D.of a sample} - \textbf{O.D.of negative control}}{\textbf{O.D.of positive control} - \textbf{O.D.of negative control}} \textbf{ x 100} \quad \textbf{…….(xvi)}$$

Where, OD samples, OD100 and OD0 are the optical density (OD) of the samples, positive control (Triton-X, 100% hemolysis) and negative control (PBS, 0% hemolysis), respectively.

References:

[1] R.R. Lorenzo, H.R. Fryer, T. Bedford, E.Y. Kim, J. Archer, S.L.K. Pond, Y.S. Chung, S. Penugonda, J.G. Chipman, C.V. Fletcher, T.W. Schacker, M.H. Malim, A. Rambaut, A.T. Haase, A.R. McLean, S.M. Wolinsky, Nature, 551 (2017) E10.

[2] R.K. Roeder, Mechanical Characterization of Biomaterials." Characterization of Biomaterials 3 (2012) 49-104.

[3] H.K. Cammenga, M. Epple, Basic Principles of Thermoanalytical Techniques and Their Applications in Preparative Chemistry, Angewandte Chemie International Edition in English 34 (1995): 1171-1187.

[4] P-S Huang, Po, S.E. Boyken, D. Baker, The Coming of Age of De Novo Protein Design, Nature, 537 (2016): 320-327.

[5] T. Kokubo, H. Takadama, How useful is SBF in predicting in vivo bone bioactivity?, Biomaterials 27 (2006) 2907–2915.

[6] A.A. Prabhu, Effect of yeast fermentation on nutraceutical and antioxidant propertiesof rice bran, International Journal of Agricultural and Food Science, 4 (2014) 59-65.

[7] D.J. Titus, T. Johnstone, N.H. Johnson, S.H. London, M. Chapalamadugu, D. Hogenkamp, K.W. Gee, C.M. Atkins, Positive allosteric modulation of the α7 nicotinic acetylcholine receptor as a treatment for cognitive deficits after traumatic brain injury, PloS one, 14 (2019) e0223180.

[8] C. Berthomieu, R. Hienerwadel, Fourier transform infrared (FTIR) spectroscopy. Photosynthesis research, 101 (2009) 157–170.

[9] R.F. Goldstein, S.K. Abell, S. Ranasinha, M. Misso, J.A. Boyle, M.H. Black, N. Li, G. Hu, F. Corrado, L. Rode, Y.J. Kim, M. Haugen, W.O. Song, M.H. Kim, A. Bogaerts, R. Devlieger, J.H. Chung, H. J. Teede, Association of Gestational Weight Gain With

Maternal and Infant Outcomes: A Systematic Review and Meta-analysis. JAMA, 317(2017), 2207–2225.

[10] R.K. Varshney, I.D. Godwin, T. Mohapatra, J.D.G. Jones, S.R. McCouch, A SWEET solution to rice blight. Nature biotechnology, 37 (2019) 1280–1282.

[11] S.K.S. Hossain, S. Yadav, S. Majumdar, S. Krishnamurthy, R. Pyare, P. K. Roy, A comparative study of physico-mechanical, bioactivity and hemolysis properties of pseudo-wollastonite and wollastonite glass-ceramic synthesized from solid wastes, Ceramics International, 46 (2020) 833-843.